De novo PADI4-mediated citrullination of histone H3 stimulates HIV-1 transcription

Luca Love[1,*], Bianca B Jütte[1,*], Birgitta Lindqvist[1], Naomi Ann Thomas[1], Oscar Kieri[2,3], Piotr Nowak[2,3], J Peter Svensson[1]

[1] Department of Biosciences and Nutrition, Karolinska Institutet, Huddinge, Sweden

[2] Division of Infectious Diseases, Department of Medicine Huddinge, Karolinska Institutet, Huddinge, Sweden

[3] Department of Infectious Diseases, Karolinska University Hospital, Stockholm, Sweden

*These authors contributed equally

Correspondence to JPS (peter.svensson@ki.se)

Highlights:

- The PADI4 enzyme stimulates HIV-1 transcription during T cell activation.
- PADI4 citrullinates histone H3 at the HIV-1 promoter upon T cell activation and inhibiting PADI4 reduces HIV-1 reactivation in *ex vivo* CD4 T cells from people living with HIV-1.
- H3cit is mostly found at gene promoters, and productive HIV-1 proviruses are more likely than latent or reactivatable proviruses, to integrate in chromatin susceptible for citrullination.
- H3cit prevents latency establishment by interfering with the binding of HP1α to H3K9me3.

Abstract

HIV-1 infection establishes a reservoir of long-lived cells with integrated proviral DNA that can persist despite antiretroviral therapy (ART). The mechanisms governing the transcriptional regulation of the provirus are complex and incompletely understood. Here, we investigated the role of histone H3 citrullination, a post-translational modification catalyzed by protein-arginine deiminase type-4 (PADI4), in HIV-1 transcription and latency. We found that PADI4 inhibition by GSK484 reduced HIV-1 transcription after T cell activation in *ex vivo* cultures of CD4 T cells from viremic and ART treated people living with HIV-1 (PLWH). The effect was more pronounced in the viremic group. Using cell models of HIV-1 latency, we showed that PADI4-mediated citrullination of histone H3 occurred at the HIV-1 promoter upon T cell stimulation which facilitated proviral transcription. Citrullination of the H3R8 residue prevented heterochromatin formation. We also demonstrated that HIV-1 preferentially integrated into genomic regions marked by H3 citrullination and that proviruses in H3 citrullinated chromatin were more transcriptionally active and less prone to latency than those in non-citrullinated chromatin. Our data reveal a novel mechanism of HIV-1 transcriptional regulation by PADI4 and H3 citrullination and suggest a potential therapeutic target for reducing the size of the latent reservoir, as an approach to cure.

Introduction

HIV-1 establishes a latent viral reservoir that persist despite active antiretroviral therapy (ART). The cells in the latent reservoir represent a heterogeneous population. Even though the cells in the latent reservoir do not produce viral particles, in many cells the HIV-1 provirus is still transcriptionally active (Yukl *et al.*, 2018; Moron-Lopez *et al.*, 2019; Dubé *et al.*, 2023). In other cells, the provirus is likely to be permanently silent, such as those integrated in epigenetically silent regions (Einkauf *et al.*, 2019; Jiang *et al.*, 2020; Lian *et al.*, 2023). Before the start of ART, HIV-1 gradually depletes the CD4 T cell population, as infected cells produce viruses before they are targeted by the immune system. However, after ART initiation, latently infected cells are selected for, since the host immune system eliminates cells expressing viral epitopes (Simonetti *et al.*, 2020). Some of these latent cells can switch between silent and active states of the provirus to avoid detection by the immune system, while maintaining the ability to spread if ART is interrupted. Latency can be induced by many factors (reviewed in Jütte, Love and Svensson, 2023), but a key determinant in long term latency is the chromatin constitution of the provirus (Jiang *et al.*, 2020; Lian *et al.*, 2023). As HIV-1 enters the genome, it is assumed to take the epigenetic profile of the chromatin where it integrates. However, the host can stably silence a locus through different mechanisms including KRAB-ZFP (KAP1) and HUSH (Tchasovnikarova *et al.*, 2015) leading to heterochromatin protein 1 (HP1) over the provirus (du Chéné

57 *et al.*, 2007). A more transient proviral inactivation is provided by lysine deacetylations (Marban *et al.*,
58 2007).
59 The proviral sequence resembles a host gene in several aspects, and the resulting transcripts are
60 initially processed similarly to human mRNAs. However, at the stage of viral particles forming, the
61 spliceosome is turned off and the unspliced viral RNA genome is transcribed to be packaged into virions
62 (Purcell and Martin, 1993). It is unclear what promotes this switch, but acetylation of viral
63 transactivator protein Tat has been proposed as one mechanism leading to loss of splicing (Berro *et*
64 *al.*, 2006). Unspliced transcripts are recognized as foreign by the HUSH complex, and specifically the
65 TASOR subunit. This recognition initiates a process of silencing the chromatin whereby the histone H3
66 lys9 is methylated (H3K9me3) to enable heterochromatin (Seczynska *et al.*, 2022).
67 Histone modifications serve as a platform for the binding of other proteins. H3K9me3 is recognized
68 and bound by the chromodomain of the α variant of HP1 (HP1α) (Bannister *et al.*, 2001). Modification
69 of arginine adjacent to lysine residues can affect the binding of chromodomain proteins that recognize
70 methylated lysines (Sharma *et al.*, 2012). Arginines can be modified by methylation or citrullination
71 (Cuthbert *et al.*, 2004). Citrullination is mediated by members of the protein-arginine deiminase (PADI)
72 family, of which PADI2 and PADI4 are found in the nucleus. PADI4 is an enzyme primarily expressed in
73 less differentiated cells and various cancer cells (Nakashima, Hagiwara and Yamada, 2002; Vossenaar,
74 2004; Chang *et al.*, 2009; Christophorou *et al.*, 2014). It citrullinates targets in the cell nucleus, including
75 several residues of histone H1, histone H3 and HP1γ (Christophorou *et al.*, 2014; Xiao *et al.*, 2017;
76 Wiese *et al.*, 2019). In endogenous retroviruses, it has been shown that H3cit8 interferes with HP1α-
77 binding to H3K9me3 (Sharma *et al.*, 2012). Changes in nuclear citrullination affect chromatin
78 accessibility of promoters (Moshkovich *et al.*, 2020). These changes in chromatin accessibility have
79 been attributed to the reduced electrostatic attraction between histones and DNA when changing
80 from positively charged arginine to neutral citrulline (Jentink *et al.*, 2023).
81 Here we describe the PADI4-mediated citrullination effect on HIV-1 transcription from the latent
82 reservoir. We show that, especially before ART is initiated, *de novo* histone H3 citrullination
83 accompanies HIV-1 transcription during cell activation and prevents proviral latency establishment.
84

85 ## Results

86 **PADI4 stimulates HIV-1 transcription after cell stimulation in cells from viremic ART naïve people**
87 **with HIV-1**

88 To test the hypothesis that citrullination affects the latent HIV-1 provirus in reservoir cells from PLWH,
89 we recruited 30 study participants to a clinical study. Given the known effect of PADI4-mediated
90 histone citrullination on heterochromatin (Sharma *et al.*, 2012; Christophorou *et al.*, 2014) together
91 with the observation that the reservoir with intact provirus becomes heterochromatic with time

92 (Lindqvist *et al.*, 2020; Lian *et al.*, 2023), we included two groups in our cohort. Firstly, viremic study
93 participants (n=14) and secondly, participants with long-term (>6 years) ART suppressed viremia
94 (<50c/ml)) (n=17). The study participants were matched across various characteristics, with the
95 exceptions being their plasma viremia levels and ART status (Table S1). CD4 T cells were isolated from
96 peripheral blood. The cells were activated by phorbol-12-myristate-13-acetate and ionomycin (PMAi)
97 after treatment with PADI4 inhibitor GSK484 or mock treatment. The intact HIV-1 reservoir was
98 measured using Intact proviral DNA assay (IPDA) (Bruner *et al.*, 2019). Cell-free RNA was measured by
99 the amount of intact virus RNA in the supernatant (Martin *et al.*, 2022). For cell-associated RNA, the
100 LTR region and the multiply spliced RNA was investigated.
101 In the entire cohort, GSK484 reduced the *ex vivo* HIV-1 activation based on cell-free RNA (Fig 1A). Upon
102 stratification between viremic and ART suppressed study participants, it was clear that cell activation
103 induced a release of intact viral particles only in cells from viremic study participants. This release was
104 dependant on H3cit as it was abolished in cells treated with GSK484. Activation of cells from the ART
105 treated study participants did not result in release of intact viruses (Fig 1B). This difference was not a
106 consequence of differences in numbers of infected cell as the intact HIV-1 reservoir was similar
107 between the two groups (Fig 1C). The cell-associated RNA from the LTR transcripts showed that both
108 groups had a clear proviral activation after PMAi-stimulation, significantly reduced in viremic samples
109 pre-exposed to GSK484 (Fig 1D). Multiply spliced processed RNA (Tat-Rev) was induced by PMAi
110 activation in cells from ART suppressed study participants only (Fig 1E), implying involvement of Tat in
111 the latency reversal process. A lack of mRNAs encoding Tat in activated cells from viremic study
112 participants suggests that latency reversal in these cells was Tat-independent. As the effect of GSK484
113 was most strongly associated with viremic study participants, we quantitated the levels of *PADI4*. We
114 observed that the expression of *PADI4* varied considerably in the cohort, but there was no difference
115 between *PADI4* expression in resting CD4 T cells from viremic or ART suppressed study participants
116 (Fig 1F).
117 This data show that PADI4 influences HIV-1 latency reversal in cells from people living with HIV-1,
118 particularly before the initiation of ART.
119
120 **PADI4 facilitates HIV-1 transcription after cell stimulation in cell models**
121 To investigate mechanisms underlying the effects of PADI4 inhibition on HIV-1 proviral activation, we
122 used established cell models of HIV-1 latency. The J-lat clone 5A8 is a Jurkat-derived cell line with a
123 single copy of a reporter HIV-1 integrated in an intron of the *MAT2A* locus. Proviral expression can be
124 tracked by flow cytometry or microscopy as the sequence for *nef* is replaced by *gfp* (Jordan, Bisgrove
125 and Verdin, 2003; Sakane *et al.*, 2011). To test the selectivity of PADI enzymes for the effect on HIV-1

126 transcription, cells were exposed to three different PADI inhibitors: pan-PADI inhibitor Cl-amidine,
127 PADI2-specific CAY10723, and PADI4-specific GSK484. The effect was measured by flow cytometry
128 after 24 h exposure. The PADI inhibitors alone had no effect on HIV-1 latency reversal (Fig 2A). When
129 cells were exposed to PADI inhibitors in combination with PMAi to stimulate the cells, Cl-amidine and
130 especially GSK484 resulted fewer GFP-positive cells (Fig 2A). We also compared the effect of GSK484
131 with GSK106, an inactive control of GSK484 control, showing that GSK484 reducing the level of HIV-1
132 reactivation compared to GSK106 (Fig S1A). This suggests that citrullination by PADI4 is part of the HIV-
133 1 latency reversal mechanism. CAY10723 resulted in no significant decrease in HIV reactivation when
134 the cells were activated with PMAi. PADI4 is known to be expressed in neutrophils (Asaga *et al.*, 2001),
135 but the gene is weakly expressed in most differentiated cell types. In our cells, we verified that PADI4
136 was expressed, although at low basal level (Fig 2B) (1,700 copies/10 ng RNA). Upon cell stimulation,
137 PADI4 expression was increased (Fig 2B). To understand the kinetics of the GSK484 effect, we set up a
138 time course experiment and observed that the PADI4 inhibition led to a lower plateau of proviral
139 activation although the kinetics were similar (Fig 2C). This is consistent with a subpopulation of cells
140 being affected by PADI4 inhibition. To eliminate the possibility that the drugs are differently
141 inactivated, we also performed a pulse experiment with PMAi and GSK484 present for one hour and
142 then washed out. The results were similar between a pulse or continuous exposure (Fig 2C).
143 In the nucleus, PADI4 citrullinates many targets, including histone H3. As observed previously (Sharma
144 *et al.*, 2012), H3cit was induced within an hour after cell activation. This induction is not observed after
145 PADI4 inhibition (Fig 2D). As expected from the stable nature of the H3cit modification, GSK484
146 prevents *de novo* citrullination but it does not reduce H3cit in a short time period (Fig 2D).
147 Stimulating T cells effectively reverses HIV-1 latency. To test if the decreased proviral activation could
148 be explained by GSK484 affecting T cell activation, we determined the abundance of the surface
149 markers CD69 (early activation) and CD25 (late activation). CD25 was not affected by PADI4 inhibition,
150 but for CD69, we observed a slight increase after GSK484 exposure (Fig 2E,F). This is unlikely to explain
151 the effect of reducing HIV-1 transcription though, as T cell activation stimulates latency reversal. The
152 GSK484 effect on cell proliferation was measured by Ki-67 expression, which remained unaffected by
153 PADI4 inhibition (Fig 2G).
154 To confirm a more general role of PADI4 in HIV-1 latency reversal, we inhibited PADI4 by GSK484 in a
155 K562-derived HIV-1 latency model (Besnard *et al.*, 2016). In K562-lat cells, the PADI4 gene was
156 expressed (48 copies/10 ng RNA), although at a lower level than in 5A8. This K562-lat cell line is
157 polyclonal with respect to HIV-1 integration sites. As observed for the 5A8 cell line, PADI4 inhibition
158 resulted in reduced PMAi-induced HIV-1 activation (Fig 2H).
159
160 **Citrullinated histone H3 at the HIV-1 provirus stimulated latency reversal**

161 We next sought to determine if histone H3 on the HIV-1 provirus is citrullinated during latency reversal.
162 To simultaneously detect H3cit and the effect on HIV-1 activation in single cells, we performed the
163 PLA-ZFP assay where the proviral promoter is marked with an engineered zinc-finger protein (ZFP)
164 (Wang *et al.*, 2014; Lindqvist *et al.*, 2022). This ZFP was introduced into 5A8 cells, to generate the 1C10
165 cells, with the proviral promoter marked by the protein. The basal level of H3cit at the HIV-1 promoter
166 was elevated after cell stimulation (Fig 3A). This effect did not occur in the presence of GSK484,
167 confirming a base level of H3cit that is augmented by *de novo* PADI4-mediated citrullination at the HIV-
168 1 locus. As expected from previous flow cytometry measurement, GSK484 reduced the GFP signal in
169 this fluorescent microscopy readout (Fig 3B).
170 We measured the influence of citrullination at different H3 residues. Three different arginines–H3R2,
171 H3R8 and H3R17–were tested for citrullination (Fig 3C). Although all residues were higher after cell
172 stimulation, H3cit8 and H3cit17 were particularly affected.
173 To map the distribution of H3cit at the provirus in 5A8 cells, we applied CUT&TAG (Kaya-Okur *et al.*,
174 2019). Mapping was done using four different conditions, unstimulated or PMAi stimulated cells with
175 or without GSK484 for 24 h. In unstimulated cells, two peaks of H3cit were found at the HIV-1 LTR
176 promoter, coinciding with two nucleosomes (nuc-0 and nuc-1) surrounding the transcription start site
177 (Fig 3D). Upon stimulation, the nuc-0 peak shifted upstream, to the NF-κB binding site and the nuc-1
178 peak disappeared. GSK484 weakened this effect. PMAi induced activation is known to shift or evict
179 nuc-1 of the HIV-1 promoter (Van Lint *et al.*, 1996). Inhibition of PADI4-mediated citrullination has
180 previously been associated with nucleosome repositioning (Moshkovich *et al.*, 2020). To confirm the
181 repositioning by GSK484, we performed a DNA protection assay (Conrad *et al.*, 2017). As expected
182 from a redistribution of nucleosomes after GSK484 exposure, the AflII site is unprotected, even without
183 cell stimulation (Fig 3E).
184
185 **Genome-wide H3cit is stably found at most promoters**
186 As a genome-wide distribution of H3cit was not available, we performed Cut&Tag to determine the
187 extent of H3cit in 5A8 cells. Peak calling using MACS2 identified mostly narrow H3cit peaks with a
188 median of 749±20 bp (Fig 4A). Mapping revealed that most (55.4%) H3cit was found at or close to
189 genes (Fig 4B). Aligning the peaks to the transcription start sites of all genes showed that H3cit was
190 predominantly found at promoters, and some in the early coding region (Fig 4C). This global H3cit
191 pattern appears to be stable, as this pattern was not affected by cell stimulation by PMAi or PADI4
192 inhibition by GSK484 (Fig S1B).
193 To relate the H3cit pattern to the distribution of other chromatin marks, we performed a ChromHMM
194 analysis (Ernst and Kellis, 2017). As expected, the genome-wide H3cit distribution clustered together

195 with histone marks found at open regions of the genome, such as H3K4me3, H3K27ac and H3K4me1
196 that are found either at promoters of enhancers. The H3cit pattern matched most closely with that of
197 H3K4me3 (Fig 4D). Both H3cit and H3K4me3 are stable marks, associated with open regions, but not
198 necessarily active gene expression (Santos-Rosa *et al.*, 2002; Howe *et al.*, 2017). On the other hand,
199 marks of heterochromatin such as H3K9me3 and H3K27me3 were clustered away from H3cit, as well
200 as H3K36me3, a mark internal to genes where transcription initiation is blocked (Bannister *et al.*, 2005).
201

202 **Productive HIV-1 integrates in H3cit chromatin**

203 Next, we sought to determine the role of H3cit in initial integration of the HIV-1 sequence. We
204 compared the genome-wide map of H3cit to previous integration site data, stratified on the fate of the
205 provirus (Battivelli *et al.*, 2018). As expected from H3cit being found in permissive regions of
206 decondensed chromatin, HIV-1 was found in regions with H3cit (Fig 4E). Interestingly, H3cit is most
207 often found at integration sites of productive proviruses. Less H3cit is found at latent or latent
208 reactivatable proviruses, implying that the H3cit structure is resistant to silencing, as previously
209 suggested for HERVs (Sharma *et al.*, 2012).
210

211 **H3cit takes part in activity of T cell receptors genes**

212 No gene set terms were significantly enriched in within the genes associated with H3cit. However, we
213 found 80 genes where new H3cit is formed after PMAi, and 145 genes where the activation-induced
214 citrullination is blocked by GSK484. The overlap is significant as 61 genes are found in both lists (Fisher's
215 exact test, $p<10^{-15}$). Two clusters of gene sets are significantly enriched: 1) "T-cell receptor", "adaptive
216 immunity", and 2) "citrullination" and "nucleosomes". Upon closer inspection of these, we do however
217 note that the gene set "Genes regulated by T cell activation" gains H3cit just upstream of the TSS after
218 T cell activation. This effect is abolished by GSK484 (Fig 4F).
219 It has previously been reported that the TNFα promoter is citrullinated after cell stimulation (Sharma
220 *et al.*, 2012). In agreement, we also observed *de novo* H3cit at the TNFα TSS after cell stimulation. This
221 effect was completely abolished in the presence of GSK484 (Fig 4G). This demonstrates the possibility
222 of several roles of H3cit in the cell during T cell activation.
223

224 ***de novo* H3cit has a general effect on HIV-1 transcription, but not through Tat or acetylation**

225 To test if the effect on the observed loss of GFP in GSK484 treated cells was a result of reduced
226 transcription or a subsequent process, we extracted RNA from the PMAi induced 5A8 cells. HIV-1
227 produces both spliced and unspliced transcripts as to create infectious viruses (Purcell and Martin,
228 1993). We tested the effect of GSK484 on short initiated (5´-LTR), early elongated unspliced (Gag),

229 multiply spliced (Tat-Rev), and late elongated (GFP) transcripts. These transcript types were equally
230 reduced by 30% after GSK484 treatment, although significance was only reached at GFP and Tat-Rev
231 (Fig 5A).
232 We next tested if H3cit impaired Tat function. We used PLA-ZFP to detect recruitment of Tat to the LTR
233 in 1C10 cells. Tat was still recruited to the LTR after GSK484 exposure (Fig 5B)., Normally Tat is
234 responsible for augmenting the transcription. However, in single cells, the amplitude of GFP expression
235 was not affected by GSK484, but the amount of GFP+ cells, further suggesting a limited role of Tat in
236 this context. To confirm the independence of Tat, we compared J-lat cells with partial HIV-1 genomes,
237 either LTR-GFP (A72), or LTR-Tat-GFP (A2) (Jordan, Defechereux and Verdin, 2001; Jordan, Bisgrove
238 and Verdin, 2003). Both cell lines were exposed to PADI-inhibitors during PMAi stimulation and showed
239 similar levels of GFP reduction after both Cl-amidine and GSK484 (Fig 5C). This is consistent with a Tat-
240 independent mechanism.
241 To further explore which host mechanisms are involved in PADI4-mediated HIV-1 transcription, we
242 tested the effect of GSK484 with different latency reversal agents. In addition to PMAi, latency reversal
243 by the protein kinase C agonist Prostratin was affected by GSK484. However, latency reversal by HDAC
244 inhibitors Romidepsin and Panabinostat was not affected by GSK484 (Fig 5D). This suggests that the
245 observed effect of PADI4 is either independent from histone acetylation, or that the subset of cells in
246 which PADI4 plays a role for HIV-1 transcription does not overlap with the one activated by HDACi.
247
248 **Heterochromatin forms over the HIV-1 provirus in the absence of H3cit**
249 Given our finding that *de novo* citrullination of H3 and possibly other targets appears to prevent HIV-1
250 transcription in primary cells from PLWH as well as in several model systems, together with the
251 previous finding of H3cit preventing heterochromatin over HERVs (Sharma *et al.*, 2012), we set out to
252 study the impact of H3cit on heterochromatin formation over the HIV-1 provirus. The 5A8 cells have
253 the provirus integrated in a permissive region, and the proviral chromatin is predominantly associated
254 with active histone marks (Lindqvist *et al.*, 2022). This chromatin structure mirrors the majority of
255 proviral integration events, as HIV-1 tends to target open chromatin (Schröder *et al.*, 2002). However,
256 once ART is initiated, new infections are prevented. The immune system targets cells producing viral
257 proteins, resulting in an advantage of latently infected cells. Long-term ART results in the provirus
258 being found in epigenetically silent regions (Lian *et al.*, 2023). To replicate this epigenetic state, we
259 modified the 5A8 cells to silence the provirus. We tethered a KRAB (Krüppel Associated Box) domain
260 to the engineered ZFP that specifically recognizes the HIV-1 provirus used for the PLA experiments
261 (Lindqvist *et al.*, 2022). We introduced this KRAB-ZFP protein into the cells and selected for monoclonal
262 cell lines. We characterized two clones in particular, 2C10 with the ZFP-KRAB, and 1C10–a control cell
263 line with only the ZFP construct. In the 2C10 cells, H3K9me3 at the promoter was confirmed by ChIP

264 (Fig 6A). The HIV-1 inducibility after 24 h PMAi stimulation was lower in 2C10 compared to the control
265 5A8 clone 1C10 (Fig 6B). As expected from less HIV-1 reactivation, the recruitment of Tat was less
266 significant in the 2C10 cells (Fig 6C). Among the cells that still had inducible HIV-1, GSK484 further
267 reduced the reactivation.
268 We hypothesized that *de novo* citrullination of the HIV-1 promoter prevents HP1α binding and
269 functional heterochromatin formation, despite occurrence of H3K9me3. From a previous study
270 (Lindqvist et al 2022), we know that following activation H3K9me3 levels increase at the HIV-1 provirus.
271 However, H3K9me3 is not sufficient to establish heterochromatin. To form functional
272 heterochromatin, the H3K9me3 should be enclosed in HP1α. In HERVs, H3cit8 hinders HP1α binding
273 to H3K9me3 (Sharma *et al.*, 2012). Consequently, by activating the cells and preventing citrullination
274 by GSK484, HP1α would be given a platform to bind. We tested the recruitment of HP1α to the HIV-1
275 promoter using PLA. We found that HP1α binds specifically to HIV-1 after cell stimulation when PADI4
276 is inhibited (Fig 6D). In the 2C10 cells, where the provirus was not activated by PMAi, HP1α was not
277 found above background levels.
278

279 ## Discussion

280 In this study, we demonstrated that the *de novo* PADI4-mediated citrullination of histone H3 at the
281 HIV-1 promoter inhibits the formation of heterochromatin and promotes HIV-1 transcription following
282 cell activation. When PADI4 activity is blocked during cell activation, new citrullination of proviral
283 nucleosomes does not occur, allowing stable heterochromatin to form. Proviruses within citrullinated
284 chromatin are not epigenetically silenced. This mechanism is particularly relevant for HIV-1 proviruses
285 integrated in permissive chromatin regions, which are less prone to latency and more responsive to
286 latency reversal agents. We also provide the first genome-wide map of H3 citrullination in T cells,
287 showing that this mark is enriched at promoters and associated with permissive chromatin.
288

289 **Implications for the reservoir in people living with HIV-1**

290 We have uncovered a mechanism that begins to explain how the HIV-1 reservoir is different in chronic
291 viremia and during long term ART in PLWH. Cells continuously producing viruses undergo cytopathic
292 effects and are targeted by the immune system (Pollack *et al.*, 2017; Simonetti *et al.*, 2020). We
293 observe a mechanism that is active in viremic individuals but is not present after long term ART. The
294 latent reservoir is, at least in part, transcriptionally active (Yukl *et al.*, 2018; Lindqvist *et al.*, 2020;
295 Collora *et al.*, 2022; Dubé *et al.*, 2023). Our study highlights the heterogeneity of the reservoir,
296 particularly during chronic infection before ART. When ART is initiated, pressure to induce
297 reactivatable latent proviruses increases. The intact viruses date to the time of ART initiation (Kinloch

298 *et al.*, 2023). The state of the reservoir when ART is initiated is key for post-treatment control and a
299 potential HIV-1 cure (Gunst *et al.*, 2022). Over time an increasing fraction of the intact provirus is
300 found in heterochromatin (Lian *et al.*, 2023). Part of the reservoir is susceptible to histone acetylation
301 and can be cleared even under ART (Armani-Tourret *et al.*, 2024). Future studies are required to reveal
302 the fate of the cells with citrullination at the promoter, that cannot be epigenetically silenced after
303 ART initiation. Many of these cells are likely eliminated through cytopathic effects or immune
304 detection, unless they are cytotoxic CD4 T cells (Collora *et al.*, 2022). A subset of proviruses might
305 become latent solely as a consequence of the cell entering a resting state (Shan *et al.*, 2017), and then
306 stochastic events cause the reactivation (Hataye *et al.*, 2019). This points to the possibility of reducing
307 the fraction of the reservoir that is subject to stochastic reactivation by manipulating PADI4 during
308 initiation of ART.
309
310 **Epigenetic interplay of H3cit and other PADI4 targets**
311 H3cit is linked to active transcription and open chromatin across various cellular contexts (Sharma *et*
312 *al.*, 2012; Christophorou *et al.*, 2014; Xiao *et al.*, 2017; Wiese *et al.*, 2019). In addition to H3, PADI4
313 targets numerous proteins in the nucleus, including histone H1 and HP1γ (Christophorou *et al.*, 2014;
314 Wiese *et al.*, 2019). We cannot exclude that modifications of these proteins also play a role in the
315 phenotype we observe.
316 Here we detailed the role of H3cit8. Notably, other H3 residues can also be citrullinated, potentially
317 influencing the cell differently. The H3cit26 mark is recognized by SMARCD1, that has been suggested
318 as a link between H3cit and heterochromatin (Xiao *et al.*, 2017). In mice ES cells, H3cit26 and H3K9me3
319 do not colocalize at basal levels. However, after PADI inhibition, H3K9me3 levels appear at the sites of
320 H3cit26 (Xiao *et al.*, 2017). Arginines, which can be citrullinated, are often found adjacent to lysines,
321 key residues for epigenetic modifications. Moreover, arginine methylation and citrullination are
322 mutually exclusive (Cuthbert *et al.*, 2004). Both arginine methylation and citrullination are stable
323 histone modifications and whereas a short pulse of PADI4 inhibition is unlikely to shift the balance
324 between methylated and citrullinated arginine residues, prolonged reduced levels of PADI4 could have
325 this effect (Moshkovich *et al.*, 2020). Arginine methylation of H3 through CARM1 has a known effect
326 on HIV-1 latency (Zhang *et al.*, 2017). We conclude that PADI4 plays a balancing role in HIV-1
327 transcription, depending on both the cell type and the site of proviral integration.
328
329 **Limitations of the study**
330 Our study is confined to CD4 T cells from peripheral blood, despite the presence of the HIV-1 reservoir
331 at several other anatomical sites in the body. While our findings are grounded in clinical samples, the
332 mechanistic insights primarily derive from cell models. We were unable to track PADI4-depleted cells

333 as they reverted to latency to determine if they were prevented from subsequent reactivation. To
334 enhance the generalizability and applicability of the findings, we employed several different cell
335 models and complementary techniques. However, we were unable to test our hypothesis *in vivo* or in
336 animal models. The small sample size in parts of the test is a limitation for the generalizability.
337
338 **Conclusions**
339 Our findings reveal a novel epigenetic mechanism that regulates HIV-1 transcription and latency,
340 suggesting that PADI4 could serve as a potential therapeutic target for interventions aimed at reducing
341 the size of the latent reservoir as an approach for cure.
342

343 ## References

344 Armani-Tourret, M. *et al.* (2024) 'Selection of epigenetically privileged HIV-1 proviruses during
345 treatment with panobinostat and interferon-α2a', *Cell*, pp. S0092-8674(24)00105–3. Available at:
346 https://doi.org/10.1016/j.cell.2024.01.037.

347 Asaga, H. *et al.* (2001) 'Immunocytochemical localization of peptidylarginine deiminase in human
348 eosinophils and neutrophils', *Journal of Leukocyte Biology*, 70(1), pp. 46–51.

349 Bannister, A.J. *et al.* (2001) 'Selective recognition of methylated lysine 9 on histone H3 by the HP1
350 chromo domain', *Nature*, 410(6824), pp. 120–124. Available at: https://doi.org/10.1038/35065138.

351 Bannister, A.J. *et al.* (2005) 'Spatial Distribution of Di- and Tri-methyl Lysine 36 of Histone H3 at
352 Active Genes', *Journal of Biological Chemistry*, 280(18), pp. 17732–17736. Available at:
353 https://doi.org/10.1074/jbc.M500796200.

354 Battivelli, E. *et al.* (2018) 'Distinct chromatin functional states correlate with HIV latency reactivation
355 in infected primary CD4(+) T cells', *Elife*, 7. Available at: https://doi.org/ARTN e34655
356 10.7554/eLife.34655.

357 Berro, R. *et al.* (2006) 'Acetylated Tat regulates human immunodeficiency virus type 1 splicing
358 through its interaction with the splicing regulator p32', *Journal of Virology*, 80(7), pp. 3189–3204.
359 Available at: https://doi.org/10.1128/JVI.80.7.3189-3204.2006.

360 Besnard, E. *et al.* (2016) 'The mTOR Complex Controls HIV Latency', *Cell Host & Microbe*, 20(6), pp.
361 785–797. Available at: https://doi.org/10.1016/j.chom.2016.11.001.

362 Bruner, K.M. *et al.* (2019) 'A quantitative approach for measuring the reservoir of latent HIV-1
363 proviruses', *Nature* [Preprint]. Available at: https://doi.org/10.1038/s41586-019-0898-8.

364 Chang, X. *et al.* (2009) 'Increased PADI4 expression in blood and tissues of patients with malignant
365 tumors', *BMC Cancer*, 9(1), p. 40. Available at: https://doi.org/10.1186/1471-2407-9-40.

366 du Chéné, I. *et al.* (2007) 'Suv39H1 and HP1gamma are responsible for chromatin-mediated HIV-1
367 transcriptional silencing and post-integration latency', *The EMBO journal*, 26(2), pp. 424–435.
368 Available at: https://doi.org/10.1038/sj.emboj.7601517.

369 Christophorou, M.A. *et al.* (2014) 'Citrullination regulates pluripotency and histone H1 binding to
370 chromatin', *Nature*, 507(7490), pp. 104–108. Available at: https://doi.org/10.1038/nature12942.

371 Collora, J.A. *et al.* (2022) 'Single-cell multiomics reveals persistence of HIV-1 in expanded cytotoxic
372 T cell clones', *Immunity*, 55(6), pp. 1013-1031.e7. Available at:
373 https://doi.org/10.1016/j.immuni.2022.03.004.

374 Conrad, R.J. *et al.* (2017) 'The Short Isoform of BRD4 Promotes HIV-1 Latency by Engaging Repressive
375 SWI/SNF Chromatin-Remodeling Complexes', *Molecular Cell*, 67(6), pp. 1001-+. Available at:
376 https://doi.org/10.1016/j.molcel.2017.07.025.

377 Cuthbert, G.L. *et al.* (2004) 'Histone Deimination Antagonizes Arginine Methylation', *Cell*, 118(5), pp.
378 545–553. Available at: https://doi.org/10.1016/j.cell.2004.08.020.

379 Dubé, M. *et al.* (2023) 'Spontaneous HIV expression during suppressive ART is associated with the
380 magnitude and function of HIV-specific CD4+ and CD8+ T cells', *Cell Host & Microbe*, 31(9), pp. 1507-
381 1522.e5. Available at: https://doi.org/10.1016/j.chom.2023.08.006.

382 Einkauf, K.B. *et al.* (2019) 'Intact HIV-1 proviruses accumulate at distinct chromosomal positions
383 during prolonged antiretroviral therapy', *The Journal of Clinical Investigation*, 129(3), pp. 988–998.
384 Available at: https://doi.org/10.1172/JCI124291.

385 Ernst, J. and Kellis, M. (2017) 'Chromatin-state discovery and genome annotation with ChromHMM',
386 *Nature Protocols*, 12(12), pp. 2478–2492. Available at: https://doi.org/10.1038/nprot.2017.124.

387 Gunst, J.D. *et al.* (2022) 'Early intervention with 3BNC117 and romidepsin at antiretroviral treatment
388 initiation in people with HIV-1: a phase 1b/2a, randomized trial', *Nature Medicine*, 28(11), pp. 2424–
389 2435. Available at: https://doi.org/10.1038/s41591-022-02023-7.

390 Hataye, J.M. *et al.* (2019) 'Principles Governing Establishment versus Collapse of HIV-1 Cellular
391 Spread', *Cell Host & Microbe*, 26(6), pp. 748-763.e20. Available at:
392 https://doi.org/10.1016/j.chom.2019.10.006.

393 Howe, F.S. *et al.* (2017) 'Is H3K4me3 instructive for transcription activation?', *BioEssays*, 39(1), pp. 1–
394 12. Available at: https://doi.org/10.1002/bies.201600095.

395 Huang, D.W., Sherman, B.T. and Lempicki, R.A. (2009) 'Systematic and integrative analysis of large
396 gene lists using DAVID bioinformatics resources', *Nature Protocols*, 4(1), pp. 44–57. Available at:
397 https://doi.org/10.1038/nprot.2008.211.

398 Jentink, N. *et al.* (2023) 'Cryoelectron tomography reveals the multiplex anatomy of condensed
399 native chromatin and its unfolding by histone citrullination', *Molecular Cell*, 83(18), pp. 3236-
400 3252.e7. Available at: https://doi.org/10.1016/j.molcel.2023.08.017.

401 Jiang, C. *et al.* (2020) 'Distinct viral reservoirs in individuals with spontaneous control of HIV-1',
402 *Nature*, 585(7824), pp. 261–267. Available at: https://doi.org/10.1038/s41586-020-2651-8.

403 Jordan, A., Bisgrove, D. and Verdin, E. (2003) 'HIV reproducibly establishes a latent infection after
404 acute infection of T cells in vitro', *Embo Journal*, 22(8), pp. 1868–1877.

405 Jordan, A., Defechereux, P. and Verdin, E. (2001) 'The site of HIV-1 integration in the human genome
406 determines basal transcriptional activity and response to Tat transactivation', *The EMBO journal*,
407 20(7), pp. 1726–1738. Available at: https://doi.org/10.1093/emboj/20.7.1726.

408 Jütte, B.B., Love, L. and Svensson, J.P. (2023) 'Molecular Mechanisms of HIV-1 Latency from a
409 Chromatin and Epigenetic Perspective', *Current Clinical Microbiology Reports*, 10(4), pp. 246–254.
410 Available at: https://doi.org/10.1007/s40588-023-00208-3.

411 Kaya-Okur, H.S. *et al.* (2019) 'CUT&Tag for efficient epigenomic profiling of small samples and single
412 cells', *Nature Communications*, 10(1), p. 1930. Available at: https://doi.org/10.1038/s41467-019-
413 09982-5.

414 Kinloch, N.N. *et al.* (2023) 'HIV reservoirs are dominated by genetically younger and clonally enriched
415 proviruses', *mBio*, 14(6), p. e0241723. Available at: https://doi.org/10.1128/mbio.02417-23.

416 Lian, X. *et al.* (2023) 'Progressive transformation of the HIV-1 reservoir cell profile over two decades
417 of antiviral therapy', *Cell Host & Microbe*, 31(1), pp. 83-96.e5. Available at:
418 https://doi.org/10.1016/j.chom.2022.12.002.

419 Lindqvist, B. *et al.* (2020) 'Chromatin maturation of the HIV-1 provirus in primary resting CD4+ T
420 cells', *Plos Pathogens*, 16(1), p. e1008264. Available at:
421 https://doi.org/10.1371/journal.ppat.1008264.

422 Lindqvist, B. *et al.* (2022) 'T cell stimulation remodels the latently HIV-1 infected cell population by
423 differential activation of proviral chromatin', *PLoS pathogens*, 18(6), p. e1010555. Available at:
424 https://doi.org/10.1371/journal.ppat.1010555.

425 Marban, C. *et al.* (2007) 'Recruitment of chromatin-modifying enzymes by CTIP2 promotes HIV-1
426 transcriptional silencing', *The EMBO journal*, 26(2), pp. 412–423. Available at:
427 https://doi.org/10.1038/sj.emboj.7601516.

428 Martin, H.A. *et al.* (2022) 'New Assay Reveals Vast Excess of Defective over Intact HIV-1 Transcripts in
429 Antiretroviral Therapy-Suppressed Individuals', *Journal of Virology*, p. e0160522. Available at:
430 https://doi.org/10.1128/jvi.01605-22.

431 Moron-Lopez, S. *et al.* (2019) 'Characterization of the HIV-1 transcription profile after romidepsin
432 administration in ART-suppressed individuals', *Aids*, 33(3), pp. 425–431. Available at:
433 https://doi.org/10.1097/QAD.0000000000002083.

434 Moshkovich, N. *et al.* (2020) 'Peptidylarginine Deiminase IV Regulates Breast Cancer Stem Cells via a
435 Novel Tumor Cell-Autonomous Suppressor Role', *Cancer Research*, 80(11), pp. 2125–2137. Available
436 at: https://doi.org/10.1158/0008-5472.CAN-19-3018.

437 Nakashima, K., Hagiwara, T. and Yamada, M. (2002) 'Nuclear Localization of Peptidylarginine
438 Deiminase V and Histone Deimination in Granulocytes', *Journal of Biological Chemistry*, 277(51), pp.
439 49562–49568. Available at: https://doi.org/10.1074/jbc.M208795200.

440 Pollack, R.A. *et al.* (2017) 'Defective HIV-1 Proviruses Are Expressed and Can Be Recognized by
441 Cytotoxic T Lymphocytes, which Shape the Proviral Landscape', *Cell Host & Microbe*, 21(4), pp. 494-+.
442 Available at: https://doi.org/10.1016/j.chom.2017.03.008.

443 Purcell, D.F. and Martin, M.A. (1993) 'Alternative splicing of human immunodeficiency virus type 1
444 mRNA modulates viral protein expression, replication, and infectivity', *Journal of Virology*, 67(11), pp.
445 6365–6378. Available at: https://doi.org/10.1128/JVI.67.11.6365-6378.1993.

446 Sakane, N. *et al.* (2011) 'Activation of HIV Transcription by the Viral Tat Protein Requires a
447 Demethylation Step Mediated by Lysine-specific Demethylase 1 (LSD1/KDM1)', *Plos Pathogens*, 7(8).
448 Available at: https://doi.org/ARTN e1002184 10.1371/journal.ppat.1002184.

449 Santos-Rosa, H. *et al.* (2002) 'Active genes are tri-methylated at K4 of histone H3', *Nature*, 419(6905),
450 pp. 407–411. Available at: https://doi.org/10.1038/nature01080.

451 Schröder, A.R.W. *et al.* (2002) 'HIV-1 Integration in the Human Genome Favors Active Genes and
452 Local Hotspots', *Cell*, 110(4), pp. 521–529. Available at: https://doi.org/10.1016/S0092-
453 8674(02)00864-4.

454 Seczynska, M. *et al.* (2022) 'Genome surveillance by HUSH-mediated silencing of intronless mobile
455 elements', *Nature*, 601(7893), pp. 440–445. Available at: https://doi.org/10.1038/s41586-021-04228-
456 1.

457 Shan, L. *et al.* (2017) 'Transcriptional Reprogramming during Effector-to-Memory Transition Renders
458 CD4(+) T Cells Permissive for Latent HIV-1 Infection', *Immunity*, 47(4), pp. 766-+. Available at:
459 https://doi.org/10.1016/j.immuni.2017.09.014.

460 Sharma, P. *et al.* (2012) 'Citrullination of histone H3 interferes with HP1-mediated transcriptional
461 repression', *PLoS genetics*, 8(9), p. e1002934. Available at:
462 https://doi.org/10.1371/journal.pgen.1002934.

463 Simonetti, F.R. *et al.* (2020) 'Antigen-driven clonal selection shapes the persistence of HIV-1 infected
464 CD4+ T cells in vivo', *The Journal of Clinical Investigation* [Preprint]. Available at:
465 https://doi.org/10.1172/jci145254.

466 Tchasovnikarova, I.A. *et al.* (2015) 'Epigenetic silencing by the HUSH complex mediates position-
467 effect variegation in human cells', *Science*, 348(6242), p. 1481. Available at:
468 https://doi.org/10.1126/science.aaa7227.

469 Van Lint, C. *et al.* (1996) 'Transcriptional activation and chromatin remodeling of the HIV-1 promoter
470 in response to histone acetylation', *The EMBO journal*, 15(5), pp. 1112–1120.

471 Vossenaar, E.R. (2004) 'Expression and activity of citrullinating peptidylarginine deiminase enzymes
472 in monocytes and macrophages', *Annals of the Rheumatic Diseases*, 63(4), pp. 373–381. Available at:
473 https://doi.org/10.1136/ard.2003.012211.

474 Wang, P. *et al.* (2014) 'Specific reactivation of latent HIV-1 with designer zinc-finger transcription
475 factors targeting the HIV-1 5 '-LTR promoter', *Gene Therapy*, 21(5), pp. 490–495. Available at:
476 https://doi.org/10.1038/gt.2014.21.

477 Wiese, M. *et al.* (2019) 'Citrullination of HP1γ chromodomain affects association with chromatin',
478 *Epigenetics & Chromatin*, 12(1), p. 21. Available at: https://doi.org/10.1186/s13072-019-0265-x.

479 Xiao, S. *et al.* (2017) 'SMARCAD1 Contributes to the Regulation of Naive Pluripotency by Interacting
480 with Histone Citrullination', *Cell Reports*, 18(13), pp. 3117–3128. Available at:
481 https://doi.org/10.1016/j.celrep.2017.02.070.

482 Yukl, S.A. *et al.* (2018) 'HIV latency in isolated patient CD4(+) T cells may be due to blocks in HIV
483 transcriptional elongation, completion, and splicing', *Science Translational Medicine*, 10(430).
484 Available at: https://doi.org/ARTN eaap9927 10.1126/scitranslmed.aap9927.

485 Zhang, Z. *et al.* (2017) 'Crosstalk between histone modifications indicates that inhibition of arginine
486 methyltransferase CARM1 activity reverses HIV latency', *Nucleic Acids Research*, 45(16), pp. 9348–
487 9360. Available at: https://doi.org/10.1093/nar/gkx550.

488

Acknowledgements

We are most grateful to the study participants without whom this study would not have been possible. We would also like to thank BEA, MedH flow facility, as well as Mukesh Varshney and Zhichang Huang for technical assistance. Funding: This study was supported by grants from CIMED FoUI-973749, VR 2019–00991, KI 2019-00846, Cancerfonden 190412Pj (to J.P.S.), Swedish Physicians Against AIDS Research Foundation FOb2020-0004 (to J.P.S), FOa2022-0001, FOa2023-0003 (to B.B.J.),

Author contributions

Conceptualization, L.L., J.P.S. ; investigation and validation, L.L, B.B.J., B.L., H.R., N.A.T., J.P.S.; clinical recruitment, P.N., O.K.; supervision, J.P.S.; funding acquisition, J.P.S. and B.B.J. Writing – original draft, L.L., B.B.J., and J.P.S.; review & editing, all co-authors.

Declaration of interests

The authors declare no competing interests.

Supplementary material

Table S1: Study participant characteristics

Table S2: Genes with log2 ratio>0.5 difference between DMSO and PMAi, or PMAi and PMAi, GSK484

Table S3: Primer sequences for ddPCR and ChIP.

Fig S1:

(A) 5A8 treated with PADI4 inhibitors for 24 h with GSK484, GSK199 and inactive control GSK106, GFP measured by flow cytometry (n=4-5).

(B) Metagene plot for H3cit peaks in DMSO, GSK484, and PMAi treated conditions in 5A8.

509 ## Figures

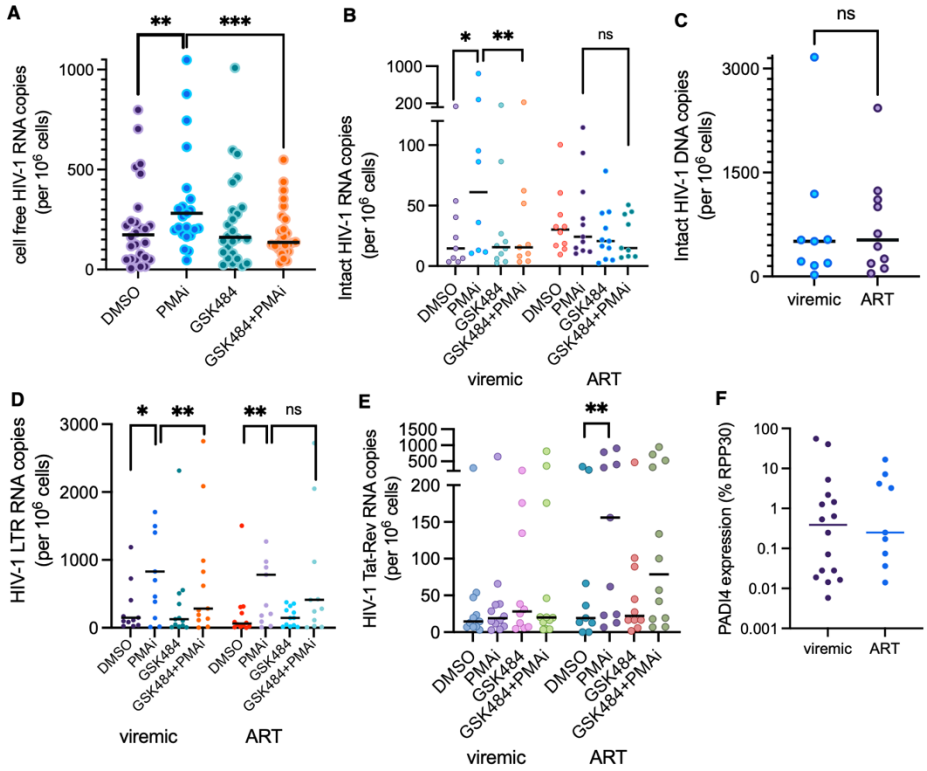

510

511 **Fig 1: PADI4 stimulates HIV-1 transcription after cell stimulation in cells from viremic people with**

512 **HIV-1.**

513 (A) Supernatant HIV-1 RNA with PMAi and GSK484 treatments from entire cohort (n=30, study

514 participant characteristics in Table S1).

515 (B) Cell associated HIV-1 RNA in cohort stratified into in viremic and long-term ART suppressed

516 groups.

517 (C) Intact HIV-1 proviral reservoir from the two groups measured by IPDA.

518 (D-E) HIV-1 5´LTR RNA (D) and Tat-Rev (E) quantified in viremic (n=14) and long-term ART suppressed

519 groups (n=17).

520 (F) PADI4 expression in the two groups normalised to RPP30.

521 All statistical tests shown are Wilcoxon matched-pairs signed rank test * $p<0.05$, ** $p<0.01$, ***

522 $p<0.001$.

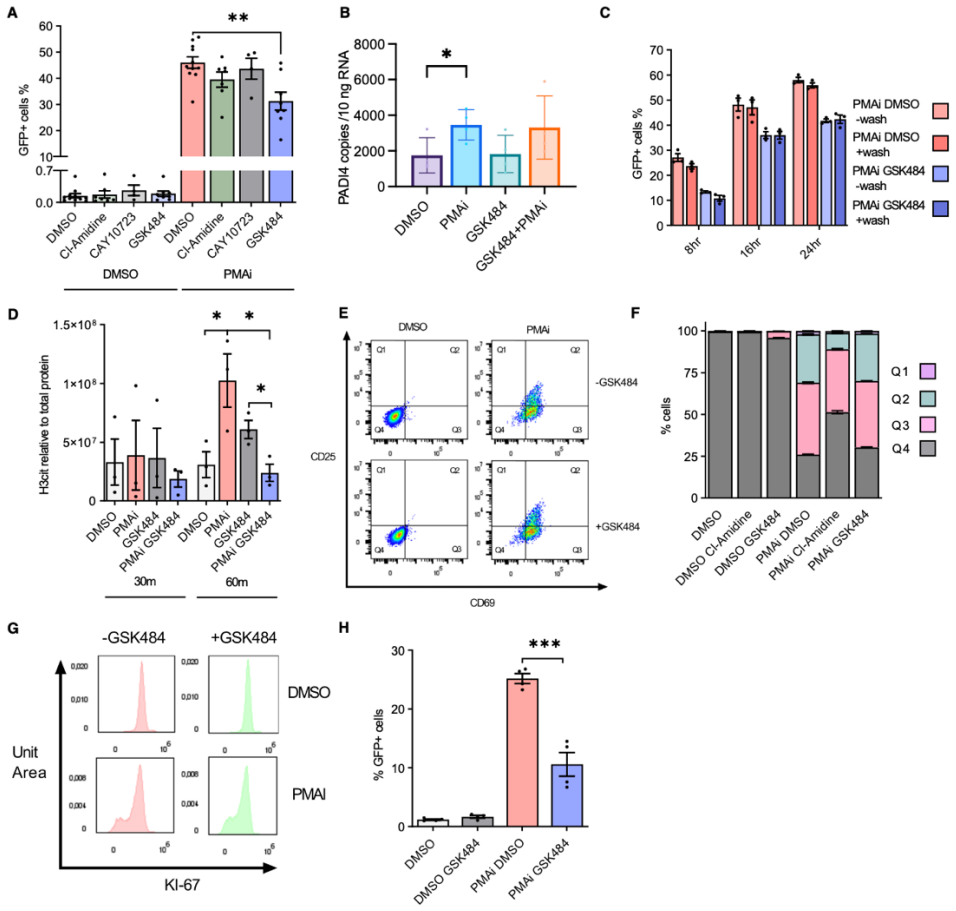

Fig 2 PADI4 facilitates HIV-1 transcription after cell stimulation in cell models.

(A) J-Lat 5A8 treated with PADI inhibitors and PMAi activation. GFP is measured by flow cytometry (n=8-11).

(B) PADI4 expression in 5A8 measured by ddPCR under PMAi and GSK484 treatment (n=4).

(C) Timecourse of 5A8 under PMAi and GSK484 treatment and flow cytometry quantification of GFP. Cells were washed and resuspended in new media without drugs after 1hr (n=3).

(D) H3cit (R2, R8,R17 residues) quantification by immunoblot in 5A8 with PMAi and GSK484 treatment at two early timepoints (n=3).

(E) T cell activation phenotype for 5A8. Cells gain CD69 during early T cell activation then CD25 during late T cell activation as shown by flow cytometry.

(F) T cell activation status of 5A8 after 24 h with different PADI4 inhibitors and PMAi activated cells (n=3).

(G) proliferation marker KI-67 staining of 5A8 treated for 24 h with PMAi and GSK484

(H) Polyclonal K562-Lat treated with PMAi and GSK484 for 24 h and quantified with flow cytometry (n=4).

Data is shown as mean ± SEM. Statistical tests shown are unpaired T tests * $p<0.05$, ** $p<0.01$, *** $p<0.001$.

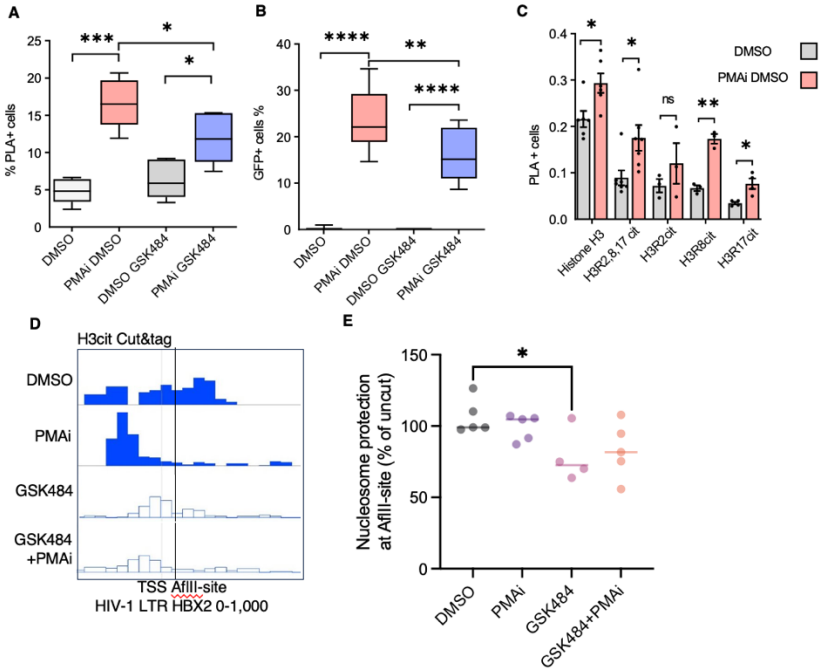

Fig 3: Citrullinated histone H3 at the HIV-1 provirus stimulated latency reversal.

(A) Quantification of H3cit at the HIV-1 promoter in 5A8 cells under PMAi and GSK484 treatment using PLA-ZFP assay (n=6).

(B) GFP levels using fluorescent microscopy from A (n=11)

(C) Quantification of different H3cit residues with PLA-ZFP in 5A8 (n=3-6)

(D) CUT&Tag seq view of total H3cit after 24 h treatment as specified.

(E) Nuc-1 accessibility assay of 5A8 (n=4-5).

Data is shown as mean ± SEM. Statistical tests shown are unpaired T tests *= <0.05 *= <0.01 *= <0.001

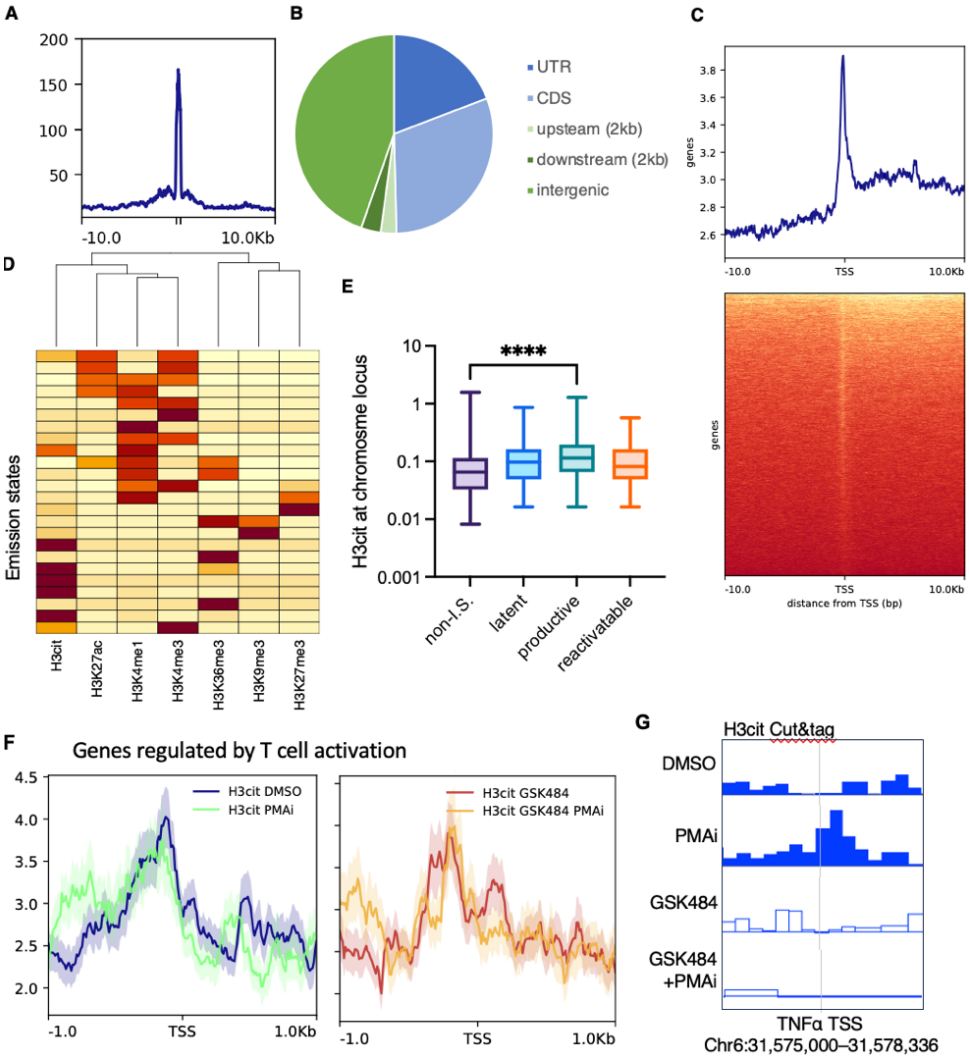

Fig 4: Genome-wide H3cit levels are stable at promoters in 5A8 with HIV-1 preferentially integrating into H3cit chromatin.

(A) CUT&Tag peak width profile.

(B) Relative enrichment of peaks in genic and non-genic regions.

(C) Metagene plot for DMSO and PMAi treated 5A8 samples

(D) ChromHMM analysis showing similarity between chromatin marks.

(E) Quantification of H3cit mapped onto known proviral integration sites with corresponding proviral activation.

(F) Metagene plot with genes regulated by T cell activation.

(G) Genome browser view of the TNFα promoter region.

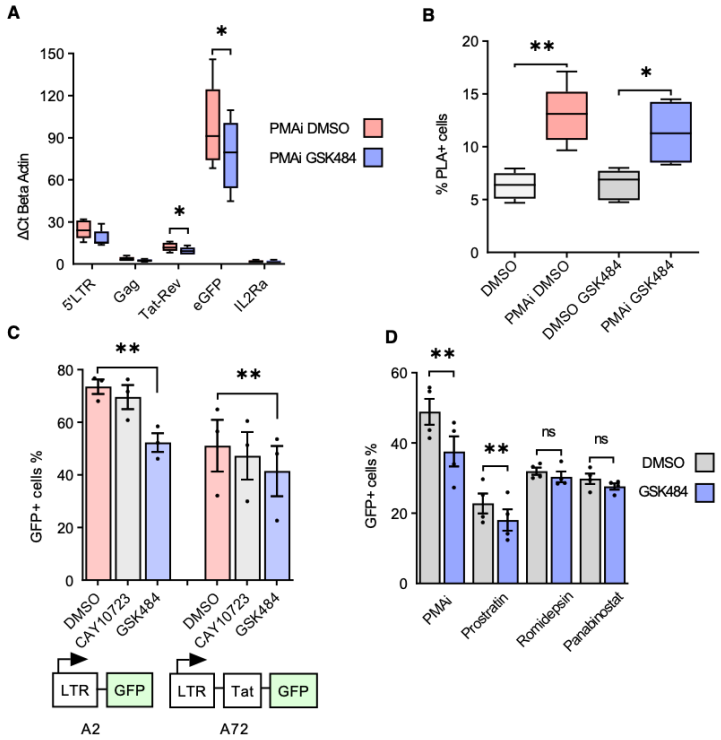

Fig 5: *de novo* H3cit has a general effect on HIV-1 transcription, but not through Tat or acetylation.

(A) RT-qPCR quantification of short initiated (5´-LTR), early elongated unspliced (Gag), multiply spliced (Tat-Rev), and late elongated (GFP) transcripts in 5A8 treated with PMAi and GSK484. Statistical tests shown are paired T tests *p<0.05 (n=5).

(B) Levels of Tat at the HIV-1 promoter in 1C10 cells with PMAi and GSK484 using PLA-ZFP assay. Statistical tests shown are unpaired T tests * p<0.05, ** p<0.01, *** p<0.001 (n=6).

(C) HIV-1 transcription of in Tat negative J-Lat A2 and Tat positive A72 cells treated with PMAi and PADI inhibitors, measured by flow cytometry. Statistical tests shown are paired T tests * p<0.05, ** p<0.01, *** p<0.001 (n=3).

(D) 5A8 cells treated with PMAi and other latency reversal agents and GSK484 (n=4).

Data is shown as mean ± SEM.

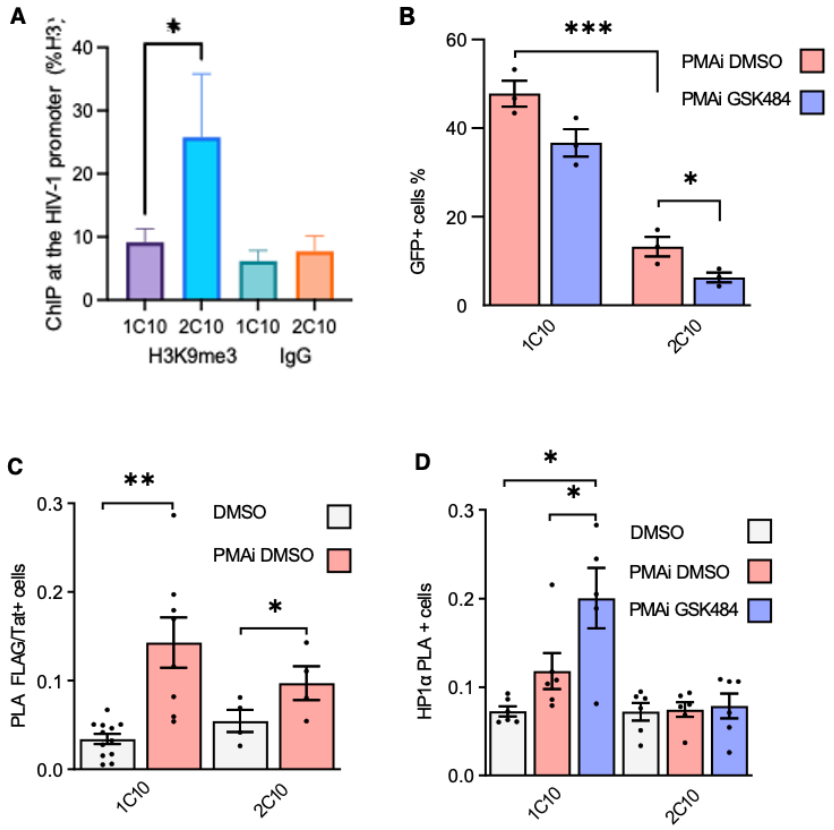

Fig 6: Heterochromatin forms over the HIV-1 provirus in the absence of H3cit.

(A) H3K9me3 at the HIV-1 locus in 1C10 and 2C10 cells measured by ChIP-qPCR. Statistical tests shown are unpaired T tests * $p<0.05$ (n=3).

(B) 1C10 and 2C10 cell HIV-1 transcription with PMAi and GSK484 treatment. Statistical tests shown are unpaired T tests * $p<0.05$, ** $p<0.01$, *** $p<0.001$ (n=3).

(C) Tat proximity to HIV-1 promoter in 1C10 and 2C10 cells with PMAi treatment. Statistical tests shown are paired T tests * $p<0.05$, ** $p<0.01$ (n=6-12).

(D) HP1α proximity to the HIV-1 promoter in 1C10 and 2C10 cells with PMAI and PMAi and GSK484 treatment (n=5-6). Statistical tests shown are paired T tests * $p<0.05$.

Data is shown as mean ± SEM.

Methods

Cell Culture and isolation

J-lat 5A8, 1C10, K562 and all primary cells were cultured in cytokine-free media (RPMI 1640 medium (Hyclone, Cat# SH30096_01), 10% FBS (Life Technologies, Cat# 10270–106), 1% Glutamax (Life Technologies, Cat# 35050), 1% Penicillin-streptomycin (Life Technologies, Cat# 15140–122)).

Primary cells were obtained from 50 ml of fresh blood from study participants (Ethical permits 2017/1138-31/4 and 2018/102-31/1). Blood samples were diluted with an equal amount of PBS and carefully overlayed on Ficoll-Paque Plus solution (Cytiva, Cat# 17144003). Centrifugation was

594 conducted at RT and 400 g for 30 minutes without brake. Resting CD4 T cells were isolated from the
595 obtained PBMCs by a two-step magnetic isolation using the Miltenyi Biotec magnetic associated cell
596 sorting (MACS) platform. For the first step, the CD4 negative cell isolation kit (Cat# 130-096-533) was
597 used according to the manufacturer's protocol. Secondly, resting CD4 T cells were negatively selected
598 with magnetic beads against the activation markers CD25, CD69 and HLA-DR.
599
600 **Cell activation**
601 CD4 T cells isolated from peripheral blood and immediately put in *ex vivo* culture. After 16 h resting,
602 cells were exposed to PADI4 inhibitor GSK484 for 3 h followed by T cell activation by phorbol-12-
603 myristate-13-acetate and ionomycin (PMAi) for 21 h. Both DNA and RNA were extracted from the cells,
604 and culture supernatant RNA was extracted to quantitate release of viral particles. DNA was extracted
605 either by Allprep (Qiagen, Cat#80204) or QIAamp DNA Mini Kit (Qiagen, Cat#51304). Viral RNA was
606 isolated by QIAamp Viral RNA Mini Kit (Qiagen, Cat#52904). The DNA was used to measure the HIV-1
607 reservoir using IPDA (Bruner *et al.*, 2019). For cell associated RNA, the LTR region and the multiply
608 spliced RNA was investigated separately. Cell-free RNA was measured by the amount of intact virus
609 RNA in the supernatant (Martin *et al.*, 2022).
610
611 **Chemicals to induce proviral activation**
612 Cells were exposed to latency reversal agents as indicated with the following concentrations used:
613 Phorbol 12-myristate 13-acetate (PMA, Sigma-Aldrich Cat# 79346) final concentration 50 ng/ml,
614 ionomycin (Sigma-Aldrich Cat# I0634) final concentration 1 µM. Ingenol-3-angelate PEP005 (Sigma-
615 Aldrich, Cat# SML1318) final concentration 12 nM, panobinostat (Cayman Chemicals, Cat#
616 CAYM13280) final concentration or 150 nM, JQ1 (Cayman Chemicals, Cat#CAYM11187) final
617 concentration 100 nM, prostratin (Sigma-Aldrich, Cat#P0077) final concentration 6 µM.
618 PADI4 inhibitor GSK484 (MCE HY-100514) was added, if applicable, at a final concentration of 10 µM.
619 Pan PADI inhibitor Cl-Amidine (Cayman Chemicals. Cat#CAYM10599) was added at a final
620 concentration of 200 µM. Inactive GSK484 and GSK199 control GSK106 (MCE HY-120343) was added
621 at a final concentration of 10 µM. Padi4 Inhibitor GSK199 (MCE HY-103058) was added at a final
622 concentration of 10 µM
623
624 **Flow cytometry**
625 Cells were stained with LIVE/DEAD Fixable Violet Dead Cell Stain (Thermo Scientific, Cat# L34955) and
626 fixed in 2% formaldehyde for 15 min. if required Flow analysis was performed on a CytoFLEX S
627 (Beckman Coulter). Individual flow droplets were gated for lymphocytes, viability, and singlets. Data
628 were analyzed by Flowjo 10.1 (Tree Star).

629 When staining for CD25 and CD69. Cells were washed with PBS (Gibco #18912014) + 0.5% BSA (FACS
630 buffer) then incubated with 1/100 CD25 (BD, Cat#555434) and CD69 1/20 (BD, Cat# 560711) antibody
631 diluted in FACS Buffer for 30 min at 4°C. Cells were then washed with 100ul of FACS buffer then
632 resuspended in 100ul FACS buffer and 1/1000 dilution of Live/dead stain (Thermo Scientific, Cat#
633 L34964) and incubated for 15 min at 4°C. Cells were washed in 100 µl FACS buffer then resuspended
634 in 2% formaldehyde PBS for 15 min in the dark at room temperature. Finally, cells were resuspended
635 in 100 µl of ice-cold PBS prior to flow cytometry.
636 When staining for KI-67 cells were washed twice with PBS and resuspended by vortexing while adding
637 ice cold 70% Ethanol. This was followed by a 1 h incubation at -20°C, three washed with FACS buffer
638 then resuspension in FACS buffer at $1x10^6$ cells/ml. 5 µl of APC anti-human Ki-67 Antibody (BioLegend,
639 CAT# 350513) in 100 µL of cell solution. This was incubated for 30 min in the dark at room temperature,
640 washed with FACS buffer then resuspended in 100 µl of ice-cold PBS prior to flow cytometry.
641
642 **KRAB domain expression in 5A8 cells**
643 The KRAB domain from pHR-SFFV-dCas9-BFP-KRAB (Addgene plasmid #46911) was cloned into plasmid
644 pHR-SFFV-ZF3-P2A-BFP using Gibson assembly (New England Biolabs Cat#E2611S) by substituting the
645 KRAB region in between the ZFP3 and P2A region.
646 The contruct was co-transfected with psPAX and pMD2.G into HEK293T cells using lipofectamine LTX
647 (Invitrogen Cat# 15338030) according to the manufacturer's instructions. 20 µL of the viral supernatant
648 was added to 180 µL of K562-Lat cell culture in a round bottom 96 well plate and spinoculated for 300g
649 for 1hr at room temperature. These were puromycin selected with 1.5 µg/ml puromycin RPMI media
650 for 5 days.
651
652 **Immunoblotting**
653 Cell pellets were lysed in lysis buffer (150 mM NaCl, 50 mM Tris, 1% Triton-X100, 1 mM orthovanadate).
654 Protein concentrations were calculated using Bradford assay (Bio-Rad Cat#5000006). Human Histone
655 H3 (citrulline R2 + R8 + R17) peptide (Abcam, Cat# ab32876) was used in a competition assay. Samples
656 were diluted to 1× Laemmli buffer (Bio-Rad, Cat# 1610747) with 10 mM DTT. Samples were heated for
657 10 min at 70°C and then loaded on a 12% Mini-protean TGX gel (Bio-Rad Cat# 4561044). The gels were
658 run for approximately 1 h at 100 V. Proteins were transferred onto a PVDF membrane (Bio-Rad, Cat#
659 1704156) and blocked in 5% skimmed milk in PBS-T for 1 h at room temperature. Afterwards, the
660 membrane was incubated at 4°C overnight with primary antibodies (1:1000) in 1% milk in PBS-T. We
661 used primary antibodies as above. After washing and addition of secondary HRP-conjugated
662 antibodies, membranes were developed using Pierce ECL Plus Western Blotting Substrate (Thermo
663 Scientific Cat# 32132). Membranes were stripped (Restore plus Western blot stripping buffer Thermo

664 Scientific Cat# 46430) and re-probed using a second set of control primary antibodies. Blots were run
665 and visualized using iBright FL1500 Imaging System (ThermoFisher).
666
667 **Chromatin immunoprecipitation**
668 ChIP-qPCR was performed using the iDeal ChIP-qPCR protocol (Diagenode, Cat# C01010180). Each ChIP
669 reaction was performed on 2×10^6 cells. Cells were fixed with 11% formaldehyde for 10 min in room
670 temperature. Sonication was performed at 30 s in eight cycles (Bioruptor Pico, Diagenode, Cat#
671 B01060010). ChIP was performed using antibody. ChIP eluates were purified with Wizard SV Gel and
672 PCR clean-up system (Promega, Cat# A9282). Primer sequences are shown in Table S2. PCR reactions
673 were performed with Powerup SYBR green master mix (2×) (ThermoFisher, Cat#A25742) using 40
674 cycles on an Applied Biosystems 7500 Fast Real-Time PCR System (ThermoFisher).
675
676 **CUT&Tag seq**
677 Version 3 CUT&Tag protocol (Kaya-Okur and Henikoff, 2020) was used as described. A 1/400 dilution
678 of Anti-Histone H3 (citrulline R2 + R8 + R17) antibody (Abcam, Cat# ab5103) was used per sample.
679 Thirteen cycles of PCR were used for amplifying the libraries. Reads were trimmed, then, mapped onto
680 the GB38 human reference genome with Bowtie2.
681
682 **Gene set enrichment**
683 Genes with log2 ratio>0.5 difference between DMSO and PMAi, or PMAi and PMAi, GSK484 were
684 selected (Table S3). The lists were analyzed using the DAVID tool (Huang, Sherman and Lempicki, 2009).
685
686 **Proximity ligation assay (PLA)**
687 Cells were adhered to coated polylysine coated microscope slides (VWR, Cat#6310107) marked with a
688 hydrophobic barrier using A-PAP pen (Histolab, Cat# 08046N) and a modified PLA protocol was
689 followed. In short, cells were washed with PBS and allowed to settle onto the polylysine slides). PLA
690 was performed according to the manufacturer's protocol (Sigma-Aldrich, cat#Duo92007) with a few
691 modifications: PLA plus and minus probes were diluted 1:20, amplification buffer (5×) was used at 10×.
692 All washes were performed in PBS. Antibodies (1:1,000) were used against Tat (Abcam Cat#43014),
693 FLAG M2 (Sigma-Aldrich Cat# F1804 lot SLCF4933), H3 (Abcam, Cat# ab1791), H3R2cit (Abcam, Cat#
694 ab176843), H3R8cit (Abcam, Cat# ab219406), H3R17cit (Abcam, Cat# ab219407),
695 H3R2cit+R8cit+R17cit (Abcam Cat# ab5103). Before DAPI staining (Life technologies, Cat# 62248) and
696 mounted with mounting medium with DAPI (Sigma-Aldrich, Cat# DUO82040), FITC-conjugated anti-
697 GFP (Abcam, Cat#ab6662) was applied (1:1000) for 1 hour at ambient temperature protected from
698 light. Coverslips (VWR, Cat# MARI0117530) were sealed onto slide with nail polish and stored at 4°C

699 overnight before imaging. Slides were imaged using a Panoramic Midi II slide scanner (3DHistech) and
700 images were exported using the CaseViewer application. Images were analyzed with ImageJ (version
701 2.0.0-rc-69/1.52) and macros developed in house. Each RGB image was separated into separate
702 channels. Based on the blue (DAPI) channel, nuclei were identified. In the red channel, spots
703 ("maxima") were detected with thresholds 6–48.
704
705 **Quantitative PCR (qPCR)**
706 RNA was extracted from cells using RNeasy plus kit (Qiagen Cat#74134) according to the manufacturers
707 instructions. Then cDNA was made using Revertaid as described (Thermo Scientific Cat#K1621). The
708 cDNA was diluted 1/10 in distilled water and used with 400 nM of each primer (final concentration)
709 and SYBR Green Master Mix for qPCR (Fisher Scientific Cat# A25742) in a Microamp Fast Optical 96
710 Well Reaction Plate (Fisher Scientific Cat#4346906). The PCRs were run using Applied Biosystems 7500
711 Fast Real-Time PCR System with 40 cycles.
712
713 **Digital droplet PCR (ddPCR)**
714 ddPCR was performed with the QX200 Droplet Digital qPCR System (Bio-Rad). Each reaction consisted
715 of 20 µL, containing 10 µL Supermix for Probes without dUTP (Bio-Rad, Cat# 1863024), 900 nM primers,
716 250 nM probe (labelled with HEX or FAM), and 8 µL undiluted cellular DNA. RT-ddPCR was used
717 according to (Martin *et al.*, 2022), using 11 µL undiluted RNA and the One-Step RT-ddPCR Advanced
718 Kit for Probes (Bio-Rad, Cat# 1864021). Droplets were generated. Emulsified PCR reactions were
719 performed with a C1000 Touch thermal cycler (Bio-Rad), with the following protocol: 95°C for 10 min,
720 followed by 40 cycles of 94°C for 30 s and 57°C for 60 s, and a final droplet cure step of 10 min at 98°C.
721 Each well was then read with a QX200 Droplet Reader (Bio-Rad). Droplets were analysed with
722 QuantaSoft version 1.5 (Bio-Rad) software in the absolute quantification mode.